Geomagnetism and Aeronomy, Vol. 39, No. 5, 1999, pp. 582–591. Translated from Geomagnetizm i Aeronomiya, Vol. 39, No. 5, 1999, pp. 46–56.

APEKS: Neutral Xenon Release Experiments

V. N. Oraevskii*, E. Y. Choueiri, V. S. Dokukin*, A. S. Volokitin*, S. A. Pulinets*, Yu. Ya. Ruzhin*, V. V. Afonin*****

** Institute of Terrestrial Magnetism, Ionosphere, and Radiowave Propagation, Russian Academy of Sciences, Troitsk, Moscow oblast, 142190 Russia*

*** Electric Propulsion and Plasma Dynamics Lab, Princeton University (EPPDyL) Princeton, USA*

**** Space Research Institute, Russian Academy of Sciences, Profsoyuznaya ul. 84/32, Moscow, 117810 Russia*

Received March 18, 1997; in final form, January 11, 1999

Abstract—The observations of broadband HF spectra and cold plasma parameters under injections of the neutral xenon jet in the ionosphere during the APEKS experiments are presented. The theoretical models of the effect of gas injections on the ambient plasma and their association with the observed anomalous ionization phenomenon are discussed.

INTRODUCTION

Alfvén [1] has proposed the critical ionization velocity (CIV) as a basic plasma physics phenomenon employed to explain various aspects of the formation of the Solar System and the ionospheres of distant planets and comets. The CIV phenomenon is a rapid (anomalous) ionization of the neutral gas that takes place when the relative velocity of the gas cloud in the magnetized plasma goes over a certain critical value, at which the kinetic energy of the atom exceeds the ionization potential. The generation of the low-frequency plasma turbulence due to the interaction of the ion beam with plasma waves is a substantial part of this phenomenon. The heating and acceleration of electrons resulting in the neutral gas ionization occur via the particle–wave and nonlinear wave–wave interactions, which are typical of this low-frequency turbulence [3, 7].

The CIV phenomenon has been intensively studied theoretically [2] and experimentally [8] for the last years. The opportunity of employing the Earth's ionosphere and magnetosphere as a perfect laboratory for experimental investigations of the CIV phenomenon is well known, and a number of active experiments with neutral gas injections have been realized: PORCUPINE [5], CONDOR [5], LIMA STAR, and *ATLAS-1* [4]. Since the interaction of the ion beam with the background plasma plays a fundamental role in the anomalous ionization of the neutral gas cloud, the rocket experiments COMBI and PORCUPINE, devoted to studying the excitation of the low-frequency turbulence by ion beams and plasma jets in the magnetized plasma, are of particular interest. Unfortunately, many details of the CIV phenomenon in these experiments remain unknown, and even the occurrence of the CIV itself is still open to question.

The APEKS (active plasma experiment of IZMIRAN) experiments with injections of xenon plasma (Xe ion beam) into the ionosphere included about twenty sessions (unplanned), when the plasma gun operated in the regime of neutral gas injection. In these cases, the kinetic energy of relative motion of Xe atoms and the ionospheric plasma exceeded the Xe ionization potential, and the necessary condition for the anomalous ionization was fulfilled. Neutral xenon was injected within the altitude range of 400–3000 km, and in contrast to other experiments (e.g. *ATLAS-1*), the experimental conditions (geomagnetic field, background velocity, angle between the gas velocity and magnetic field) significantly changed along the polar orbit of the satellite

Since studying the anomalous ionization was not planned during the APEKS, the flow rate of the neutral xenon could not exceed a nominal value of 3 mg/s. This rate is smaller by three orders of magnitude than that in the *ATLAS-1* experiment. But, in contrast to the *ATLAS-1* experiment, where the duration of each injection did not exceed 100 ms, the gas injections during the APEKS experiment lasted for several minutes. However, a relatively small mass of the injected gas apparently did not provide a complete CIV manifestation. Nevertheless, some individual physical processes constituting CIV phenomena could be detected during these experiments.

To study the processes responsible for CIV, we examined the effects of the gas injection on the HF spectra of the plasma turbulence, the spectra of accelerated electrons, and those of the electric field oscillations in the vicinity of the low-hybrid frequency. Their relation to the angle between the magnetic field and the gas flow direction was also studied when analyzing the APEKS data. The measurements obtained during this experiment indicated the specific effects of the neutral gas flow on the ambient plasma; namely, changes in the plasma density, temperature, and anisotropy, as well as changes in the vehicle potential and enhancement of the

wave activity at all frequencies, were observed in a number of cases.

Our work is presented as follows. After a brief description of the scientific facilities (Section 2), we present the data of observations of the cold plasma parameters and HF waves (Section 3). In Section 4, we present the theoretical models of interaction between the neutral cloud and plasma under the conditions of the APEKS experiment, and an analysis of the processes of preliminary gas ionization and formation of the non-equilibrium ion distribution. A quasi-linear theory of the instability of the spatially limited ion beam in the plasma and heating of electrons, as well as an additional ionization of the neutral gas and other effects accompanying the CIV phenomenon, are also considered. The last section includes the conclusions.

THE DIAGNOSTIC COMPLEX AND REGIMES OF NEUTRAL Xe INJECTIONS

The scientific facilities of the artificial satellite *Intercosmos-25* contain two electron guns with an acceleration voltage of 8 keV and a current of 100 mA, a neutral gas and Xe plasma injector with an effective current of 2–4 A, as well as detectors of the micro- and macro-parameters of the thermal and "suprathermal" plasma components, quasi-static magnetic and electric fields, and electromagnetic fields in the ELF, VLF, LF, and HF ranges. Unfortunately, some detectors did not operate during the neutral Xe injections, and data on the electron and ion distributions and low-frequency components of electric and magnetic fields are absent. Below, we briefly present detectors, the data of which are of interest for studying the anomalous ionization.

The most interesting data on one component of the electric and magnetic fields within the frequency range 0.1–10 MHz were measured with an HF wave detector. These observations are discussed further.

The parameters of the ionospheric plasma (ion density and three components of electron temperature) were measured with a KM-10 device, which uses as detectors flat nickel probes 3.5 cm in diameters. One of these probes was selected for continuous fixing of its potential with respect to the vehicle. Due to the high input impedance of the differential amplifier used, the probe potential was close to that given by a balance between the fluxes of electrons and accumulated ions. The KM-10 device provides voltage measurements of up to ±90 V, which is the limit for an amplifier. A KM-10 detector was mounted in front of the solar panels on the 1-m-long rod directed along the vehicle velocity and was outside the injected xenon (or plasma) jet.

The quasi-static magnetic field was measured by a triaxial magnetometer with a dynamic range of ±6400 nT. The data of another triaxial magnetometer integrated into the control system could be additionally used.

Neutral xenon was injected with a stationary plasma injector (UPM) in the regime without the discharge setoff. This device was mounted in the upper unit of the spacecraft in such a manner that its axis was directed into the backward hemisphere relative to the vehicle velocity and at an angle of 45° with respect to the vertical axis of the spacecraft. The neutral gas was injected in twenty sessions of operation without application of the ionization voltage for certain technical reasons. In addition, the standard regimes of UPM operation also involved 5–6 s intervals of neutral Xe injection at the beginning of each session. The kinetic energy of the relative motion of xenon atoms exceeded 20 eV, which is significantly greater than the xenon ionization potential U_I = 12–13 eV. However, the total mass of injected Xe atoms was small enough, and all manifestations of the anomalous ionization (complete CIV) were hardly observed in our experiments. Nevertheless, some physical processes belonging to the CIV phenomenon could be actually observed.

OBSERVATIONS OF THE BROADBAND HF EMISSION

Among the observational data studied, the effect of neutral gas injection is most pronounced in the results of measurements of the broadband HF spectra. The observations of HF activity are presented by the following broadband data, which show two typical cases of injection (with large and small pitch angles) and evident pitch-angle dependence. We can summarize the observed effects as follows.

The emission of HF plasma waves in the frequency range 3–10 MHz was intensified in all studied cases of neutral xenon injection (see the table) with a large (close to normal) pitch angle, namely within 85°–115°. For small pitch angles, namely, within 57°–71°, such an intensification was not observed.

Figure 1 shows typical broadband HF spectra in the frequency range 1–10 MHz measured during the neutral xenon injection in orbit 419. The signal amplitude is shown by a color (by the gradation of gray or the iridescent picture). The injection events are marked by vertical lines. The red curves present the first five harmonics of the electron cyclotron frequency. The injection was performed with large pitch angles, beginning from 94.8° at the instant of valve opening to 113° at its closing. The upper panel shows the UPM voltage time variations and indicates cycles of injector operation during the neutral gas injection.

In Fig. 1, we can see the following features of the broadband HF spectra:

(1) A wave activity is observed in a narrow band (dark stripe with gray tints) centered approximately at a frequency of 3.7 MHz, which starts at valve opening (to an accuracy of the detector time resolution) and continues until its closing. Then, the activity decays in band and amplitude.

(2) Wave activity is also observed in a wider frequency band from 8 to 10 MHz, mainly as a light stripe

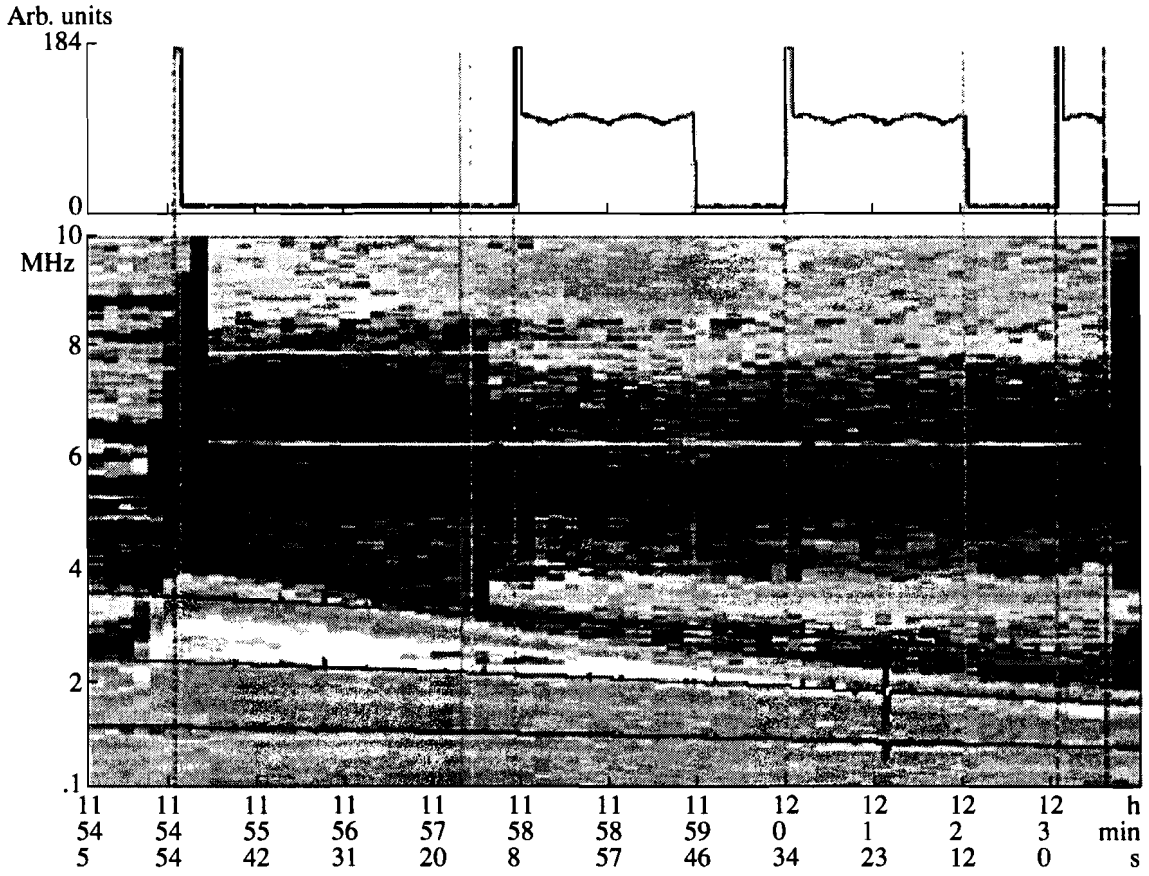

Fig. 1. Broadband HF spectra detected in the range 1–10 MHz at the neutral xenon release in orbit 419. The signal amplitude is shown by gray tints; various events of the gas release are marked by vertical lines; dark lines show the time variation in the first harmonics of the electron cyclotron frequency. The top panel presents the voltage applied to the UPM (in arbitrary units).

with darker tints. This activity exhibits the same features as in the described-above narrow band, but the emission breaks more sharply at valve closing.

(3) Both above emission bands are horizontal and do not display the time variation in the magnetic field which is shown in Fig. 1 by the harmonics of the electron cyclotron frequency.

(4) All other features are either natural ionospheric phenomena or wave activities not affected by the neutral gas injection.

It is indeed difficult to completely explain this wave activity. Since the frequencies of enhanced waves do not display changes in the magnetic field and density during the measurements, they cannot be directly associated with natural plasma frequencies. Nevertheless, it

Orbital parameters for the gas injection with the broadband HF spectra discussed

Orbit	Launch (GMT)	Altitude, km	Latitude Longitude, deg	Velocity, km/s	Pitch angle, deg	Illumination
419	Jan. 22, 1992 11:57:30	666.4	59.54 −17.75	8.01	95–113	+
490	Jan. 28, 1992 11:57:00	838.7	58.91 −8.8	7.84	95–113	+
426	Jan. 23, 1992 01:51:20	573.1	46.02 −8.898	8.1	64–71	–
496	Jan. 28, 1992 23:47:28	522.6	40.31 −29.3	8.15	57–70	–

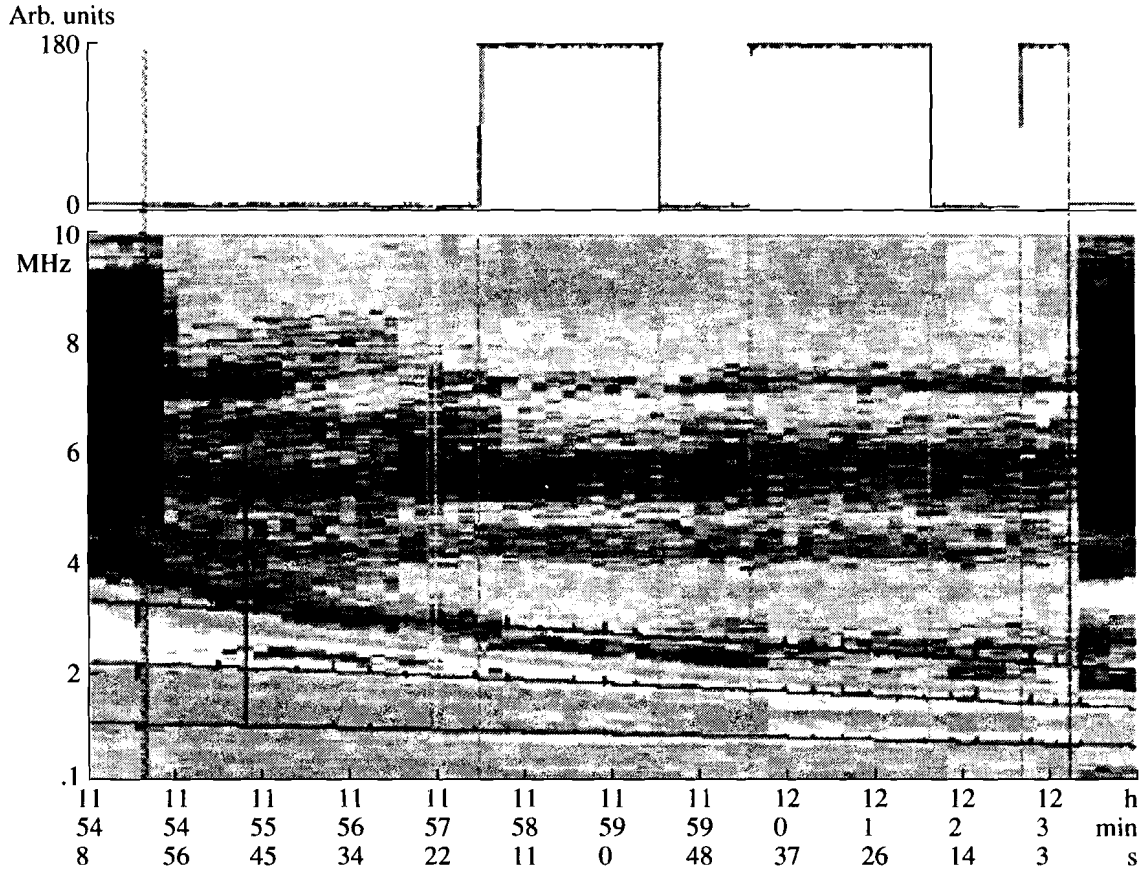

Fig. 2. Broadband HF spectra detected in the range 1–10 MHz at the neutral xenon release in orbit 490.

is obvious that their occurrence and features are well attributable to the gas injection.

Another example of broadband HF data for the injection with a large pitch angle is shown in Fig. 2. The injection was performed in orbit 490. The same comments that were made for Fig. 1 (orbit 419) are valid in this case, though a clear additional enhancement of the broadband noise is observed here over the whole spectrum, starting with the switch-on of the cathode heater and ending with the switch-off of all UPM subsystems.

Figure 3 shows an example (orbit 496) of injection with a small pitch angle. In contrast to the cases discussed above, these data do not indicate any changes in the wave activity attributable to any event associated with the neutral gas injection.

Despite the fact that the HF effects described above well correlate with the pitch angle, it is not clear whether this correlation is casual and the detected emissions controlled by other conditions, for example, by the position in orbit and background plasma parameters correlating with the pitch angle. In particular, it is noteworthy that, due to an unplanned synchronization between the motion along the polar orbit, the cycle of the solar illumination, and the program of injections, all injections with large pitch angles were performed in sunlit hours, whereas all injections with small pitch angles were carried out at night. Therefore, the solar light, rather than the pitch angle, is possibly decisive in the appearance of the above effects. The role of the sunlight in exciting broadband HF oscillations due to increasing plasma density during photoionization is worthy of studying in this case. Since the time variations in the solar radiation are small and the gas flow rate is constant during the injection, this mechanism can explain the constant frequencies of excited bands in the course of time.

Finally, we cannot rule out the role of ground-based broadcasting stations in producing the horizontal frequency bands observed in HF spectra. However, the occurrence of these bands only during injections remains open to question.

The analysis of the measurements of cold plasma parameters during the neutral gas injections do not indicate any significant changes of plasma density. Figure 4 presents the plasma density and temperature and the vehicle potential measured by the KM-10 in orbit 419. These data are free from telemetric noise and indicate rather strong variations in the plasma temperature and density as well as in the vehicle potential, which are not associated with the xenon injection. Figure 5 shows the plasma electron temperature varying in

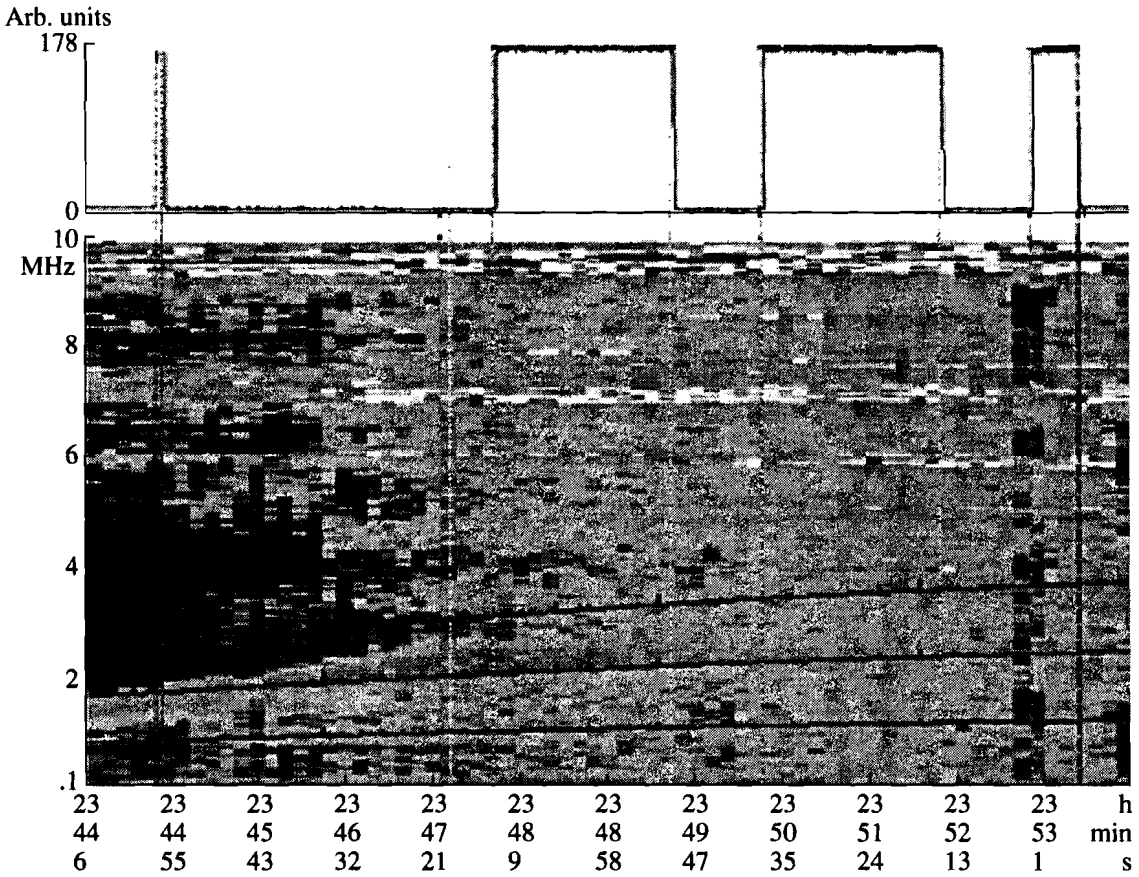

Fig. 3. Broadband HF spectra detected in the range 1–10 MHz at the neutral xenon release in orbit 496.

time along and across the magnetic field in more detail. The chronology of the UPM voltage shown in arbitrary units in the top panel permits us to compare the measurements with the UPM regimes. The behavior of the parameters is sufficiently clear, and we can argue that the density change associated with the neutral gas injection is insignificant. A peak of temperature observed tens of seconds before the gas injection, in all probability, is independent of heating and acceleration of electrons during the xenon jet interaction with ambient plasma. We can draw the same conclusions when considering the data for other orbits.

The lack of other clear manifestations of the anomalous ionization most likely results from the low stream density (small mass) of the gas injected in the APEKS experiment. Even if the conditions for ion beam instability were realized, the evolving turbulence was still much weaker than that detected by the *ATLAS-1* satellite.

DISCUSSION

For the regime of neutral gas injection, the flow rate corresponds to the plasma injection current (2–3 A) accounting for $dN_{Xe}/dt = (2–6) \times 10^{19}$ atom/s. The average stream velocity v is one–two thermal speeds (1–2 v_T) of Xe stored in the container. Though v_T is not precisely known, we can assume that $v_T \leq 10^4$ cm/s. Thus, a cloud of the neutral gas was formed around the vehicle and moved through the background plasma at a velocity of 5 ± 8 km/s. We assume that the cloud forms a spherical cone with an angle of 60° and a circular cross section. Assuming that the gas density in the spherical cone is uniform for each cross section (we can also assume a more accurate Gaussian density distribution), we can estimate the density at a distance r as

$$n_{Xe} = \frac{dN_{Xe}}{dt}\frac{1}{2\pi r^2 v_T} = 10^{15}/r^2. \quad (1)$$

Here, $dN_{Xe}/dt = (2–6) \times 10^{19}$ atom/s is the flow rate of the neutral xenon escaping with the velocity $v = v_T \leq 10^4$ cm/s. For instance, the gas density $n_{Xe} = 10^9$ and 10^7 cm^{-3} for $r = 100$ and 1000 m, respectively.

If some of the Xe atoms are ionized, the interaction of the stream of these "seeded" ions with the background plasma can initiate the anomalously rapid ionization. There are several possibilities to reach the necessary preliminary ionization: ionization by an electric discharge in an injector, ionization of Xe atoms during inelastic charge-exchange collisions with ambient plasma ions, ionization by an electron impact at colli-

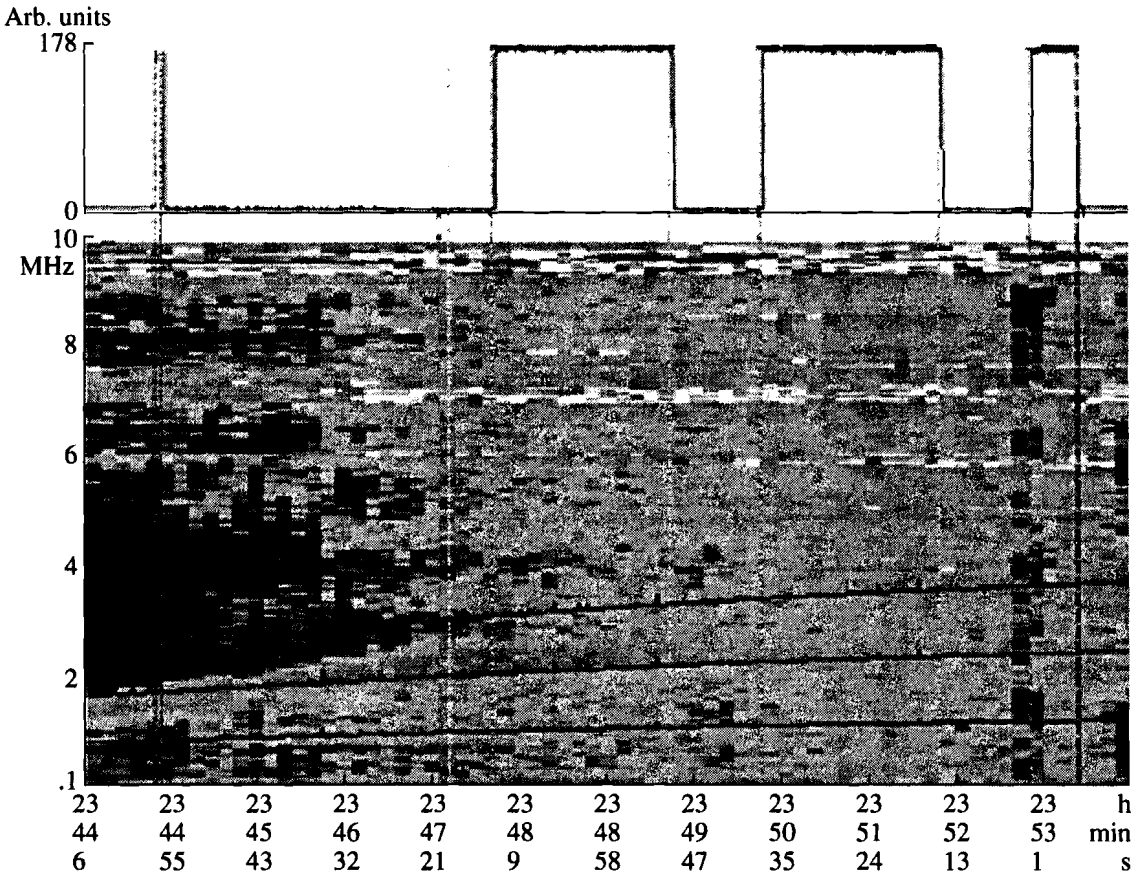

Fig. 3. Broadband HF spectra detected in the range 1–10 MHz at the neutral xenon release in orbit 496.

time along and across the magnetic field in more detail. The chronology of the UPM voltage shown in arbitrary units in the top panel permits us to compare the measurements with the UPM regimes. The behavior of the parameters is sufficiently clear, and we can argue that the density change associated with the neutral gas injection is insignificant. A peak of temperature observed tens of seconds before the gas injection, in all probability, is independent of heating and acceleration of electrons during the xenon jet interaction with ambient plasma. We can draw the same conclusions when considering the data for other orbits.

The lack of other clear manifestations of the anomalous ionization most likely results from the low stream density (small mass) of the gas injected in the APEKS experiment. Even if the conditions for ion beam instability were realized, the evolving turbulence was still much weaker than that detected by the *ATLAS-1* satellite.

DISCUSSION

For the regime of neutral gas injection, the flow rate corresponds to the plasma injection current (2–3 A) accounting for $dN_{Xe}/dt = (2–6) \times 10^{19}$ atom/s. The average stream velocity v is one–two thermal speeds (1–2 v_T) of Xe stored in the container. Though v_T is not precisely known, we can assume that $v_T \leq 10^4$ cm/s. Thus, a cloud of the neutral gas was formed around the vehicle and moved through the background plasma at a velocity of 5 ± 8 km/s. We assume that the cloud forms a spherical cone with an angle of 60° and a circular cross section. Assuming that the gas density in the spherical cone is uniform for each cross section (we can also assume a more accurate Gaussian density distribution), we can estimate the density at a distance r as

$$n_{Xe} = \frac{dN_{Xe}}{dt}\frac{1}{2\pi r^2 v_T} = 10^{15}/r^2. \quad (1)$$

Here, $dN_{Xe}/dt = (2–6) \times 10^{19}$ atom/s is the flow rate of the neutral xenon escaping with the velocity $v = v_T \leq 10^4$ cm/s. For instance, the gas density $n_{Xe} = 10^9$ and 10^7 cm^{-3} for $r = 100$ and 1000 m, respectively.

If some of the Xe atoms are ionized, the interaction of the stream of these "seeded" ions with the background plasma can initiate the anomalously rapid ionization. There are several possibilities to reach the necessary preliminary ionization: ionization by an electric discharge in an injector, ionization of Xe atoms during inelastic charge-exchange collisions with ambient plasma ions, ionization by an electron impact at colli-

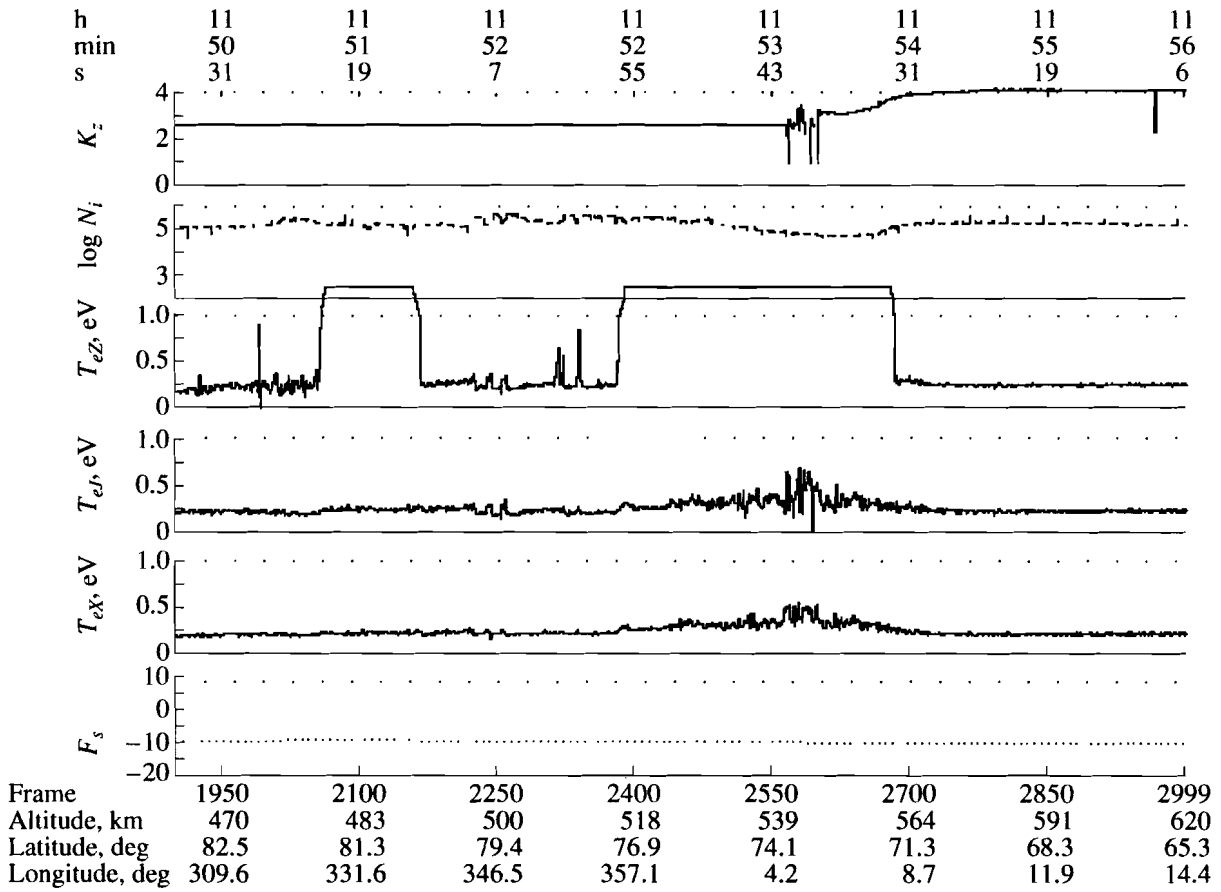

Fig. 4. The plasma density and temperature in three directions and the vehicle potential measured with the KM-10 device in orbit 419. The quantities plotted on the abscissa: (top) time; (bottom) numbers of telemetric frames and orbit parameters (altitude, latitude, and longitude).

sions with plasma electrons, and photoionization. We assume that, at least for twenty cases of neutral gas injection, the first possibility should be eliminated and we consider the efficiency of the last three processes.

Xe Ionization at Charge Exchange Collisions

The cross section of inelastic charge-exchange collisions between Xe and O^+ ions is $\sigma_{ch} \approx 2 \times 10^{-15}$, which is smaller than the cross sections of elastic collisions. We can estimate the local charge-exchange Xe ionization rate by the following formula (sign $\langle\rangle$ denotes averaging over a velocity distribution):

$$dn_{Xe^+} = \langle \sigma_{ch} n_i v \rangle n_{Xe}.$$

Taking into account that the number of injected atoms grows linearly with time, after integration in time and volume, we obtain the total number of Xe ions produced within time t at charge-exchange collisions with the plasma ions

$$\bar{N}_{Xe^+} = t \int \langle \sigma_{ch} n_i v \rangle n_{Xe} dV$$

$$= \langle \sigma_{ch} n_i v \rangle t \int^{r/v_T} \frac{dN_{Xe}}{dt} \frac{d^3 r}{r^2 v_T} \approx \langle \sigma_{ch} n_i v \rangle t \frac{dN_{Xe}}{dt} \frac{r}{v_T}$$

$$\sim \langle \sigma_{ch} n_i v \rangle \frac{dN_{Xe}}{dt} t^2 \approx 10^{15} t^2.$$

It is unlikely that the newly produced ions can be detected by the facilities mounted on a spacecraft. First, the Larmor radius of Xe ions is large ($r_L \geq 500$ m), and, second, the Xe ions never reach the vehicle detectors due to both the **[EB]** drift and the initial relative velocity.

Impact Ionization by Plasma Electrons

We can estimate the number of Xe ions produced by inelastic collisions with plasma electrons as it was done in the preceding section. However, we must take into account a significant difference; namely, that the number of electrons with an energy exceeding the ionization potential is very small at an ambient-plasma elec-

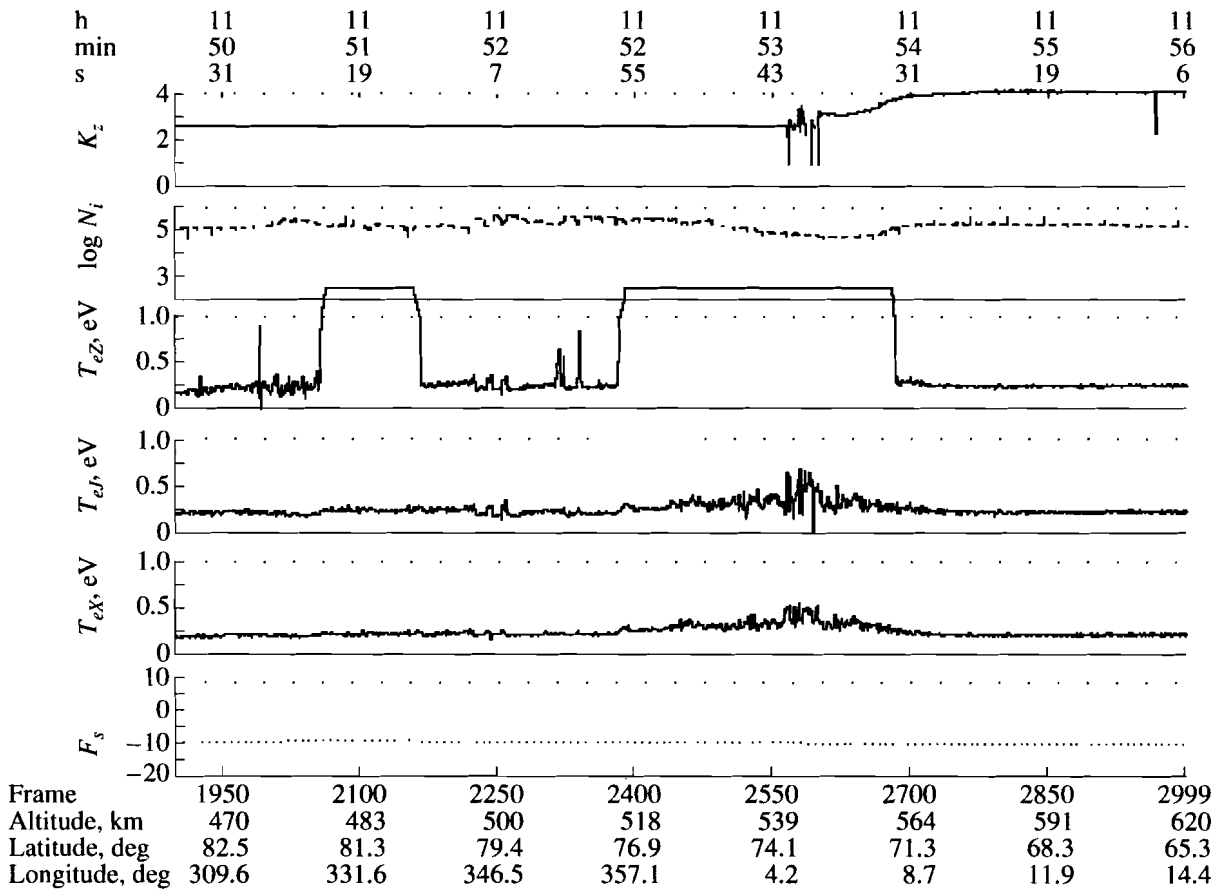

Fig. 4. The plasma density and temperature in three directions and the vehicle potential measured with the KM-10 device in orbit 419. The quantities plotted on the abscissa: (top) time; (bottom) numbers of telemetric frames and orbit parameters (altitude, latitude, and longitude).

sions with plasma electrons, and photoionization. We assume that, at least for twenty cases of neutral gas injection, the first possibility should be eliminated and we consider the efficiency of the last three processes.

Xe Ionization at Charge Exchange Collisions

The cross section of inelastic charge-exchange collisions between Xe and O^+ ions is $\sigma_{ch} \approx 2 \times 10^{-15}$, which is smaller than the cross sections of elastic collisions. We can estimate the local charge-exchange Xe ionization rate by the following formula (sign $\langle\rangle$ denotes averaging over a velocity distribution):

$$dn_{Xe^+} = \langle \sigma_{ch} n_i v \rangle n_{Xe}.$$

Taking into account that the number of injected atoms grows linearly with time, after integration in time and volume, we obtain the total number of Xe ions produced within time t at charge-exchange collisions with the plasma ions

$$\bar{N}_{Xe^+} = t \int \langle \sigma_{ch} n_i v \rangle n_{Xe} dV$$

$$= \langle \sigma_{ch} n_i v \rangle t \int^{r/v_T} \frac{dN_{Xe}}{dt} \frac{d^3 r}{r^2 v_T} \approx \langle \sigma_{ch} n_i v \rangle t \frac{dN_{Xe}}{dt} \frac{r}{v_T}$$

$$\sim \langle \sigma_{ch} n_i v \rangle \frac{dN_{Xe}}{dt} t^2 \approx 10^{15} t^2.$$

It is unlikely that the newly produced ions can be detected by the facilities mounted on a spacecraft. First, the Larmor radius of Xe ions is large ($r_L \geq 500$ m), and, second, the Xe ions never reach the vehicle detectors due to both the **[EB]** drift and the initial relative velocity.

Impact Ionization by Plasma Electrons

We can estimate the number of Xe ions produced by inelastic collisions with plasma electrons as it was done in the preceding section. However, we must take into account a significant difference; namely, that the number of electrons with an energy exceeding the ionization potential is very small at an ambient-plasma elec-

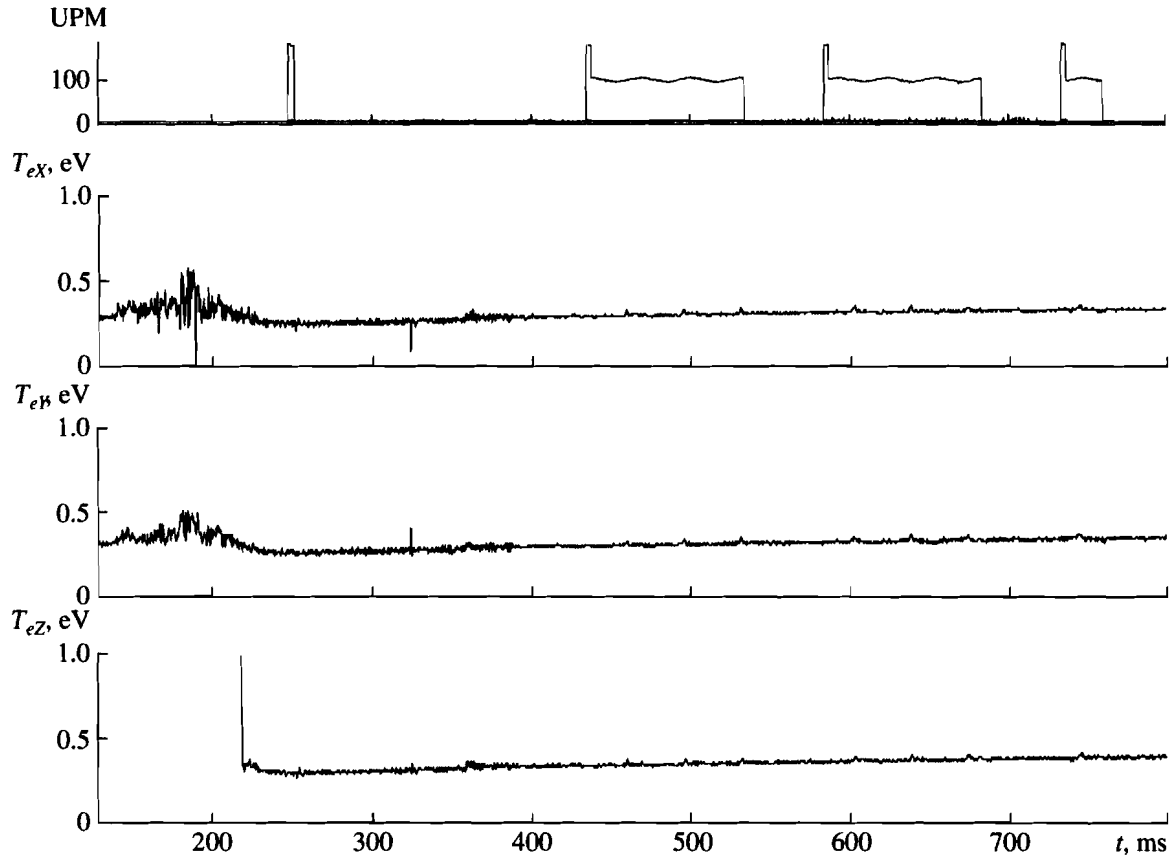

Fig. 5. The electron temperature variations (in eV) measured in three directions (along and perpendicular to the magnetic field) as a function of time elapsed from the instant t = 11:52:55. The top panel shows the variation in the voltage applied to UPM (in arbitrary units).

tron temperature of 1–2 eV. So, the effective ionization frequency is

$$\langle \sigma_{eion} n_e v \rangle \approx 10^{-16} n_e v_{T_e} \exp\left(-\frac{eU_i}{T_e}\right),$$

and the local ionization rate can be determined according to

$$dn_{Xe^+} = \langle \sigma_{eion} n_e v \rangle n_{Xe} \approx 10^{-16} n_e v_{T_e} \exp\left(-\frac{eU_i}{T_e}\right) n_{Xe}.$$

We now obtain an estimate for the total production rate of Xe ions during electron collisions

$$\bar{N}_{Xe^+} = t\int \langle \sigma_{eion} n_e v \rangle n_{Xe} dV \approx \langle \sigma_{eion} n_e v \rangle t \frac{dN_{Xe}}{dt} \frac{r}{v_T} \quad (2)$$

$$\sim 10^{-16} n_e v_{T_e} \exp\left(-\frac{eU_i}{T_e}\right) \frac{dN_{Xe}}{dt} t^2 \approx 10^{13} t^2$$

and see that this value is less than the charge-exchange ionization rate by two orders of magnitude.

Below, we shall consider the processes following the appearance of Xe ions in the ambient plasma during a neutral gas injection. However, a different process not considered above is a more efficient source of plasma disturbances and gives rise to wave generation and heating of ambient plasma electrons and creates prerequisites for the anomalous ionization. It is the reflection of ambient plasma ions at elastic collisions with the neutral gas stream, which will be considered in the next section.

Elastic Reflection of Plasma Ions Colliding with a Neutral Xenon Stream

The gas density near a Xe injector is high, and the collisions of Xe atoms with ambient plasma ions can be significant. Let us estimate the distance from an injector at which the ion free path in the neutral gas $\lambda = 1/\sigma n_{Xe}$ is smaller than or equal to this distance $r_c = \lambda$. For the cross section of elastic collisions $\sigma \sim 10^{-14}$ cm^2, this distance is smaller than 10–20 cm, and virtually all flow of ionospheric plasma through the beginning of a Xe cloud will be stopped (or reflected and scattered) due to collisions with neutrals.

Elastic collisions can affect the ambient plasma up to distances of 100–300 cm. The probability of scatter-

ing the ionospheric ion on its path dl in the Xe cloud is $\sim dl/\lambda$. Then, the flux of ionospheric ions $\sim\langle n_i v\rangle$ loses

$$d\bar{N}_i = \langle n_i v\rangle dS\frac{dl}{\lambda} = \langle n_i v\rangle \sigma n_{Xe} dS dl$$

particles per second at a distance dl, while passing through the dS section of a Xe cloud. The total number of reflected ionospheric ions per second is determined from the equation

$$\bar{N}_i = \langle n_i v\rangle \int \sigma n_{Xe} dS dl$$

$$= \langle n_i v\rangle \sigma \int n_{Xe} dV = \langle n_i v\rangle \sigma N_{Xe},$$

where N_{Xe} is the total number of injected Xe atoms. Thus, for typical parameters $n_i \approx 10^4$ and $v \approx v_{sc} \approx 8 \times 10^6$, the total flux of O^+ ions scattered in time t equals

$$\bar{N}_i = \langle n_i v\rangle \sigma \frac{dN_{Xe}}{dt} t \quad (3)$$

$$\approx 10^4 \times 8 \times 10^6 \times 10^{-14} \times 6 \times 10^{19} \approx (10^{15}\text{–}10^{16})t.$$

The energy of oxygen ions is virtually constant at collisions due to the great difference between O^+ and Xe ion masses. Therefore, to a first approximation, we can consider the distribution of reflected ions as isotropic in the reference system of an Xe cloud (satellite). The ionospheric ions reflected by a neutral cloud are magnetized and continue the [**EB**] drift in this system together with the main flow. At the same time, in the reference system of ionospheric plasma at distances less than the Larmor ion radius, the reflected ions form the flux of warm ions with the drift velocity $\sim v_{sc}$ and velocity spread $\sim\left(\frac{1}{2}-\frac{1}{3}\right)v_s$.

A certain portion of the flux of ionospheric ions is captured by the neutral Xe cloud. The density of ionospheric oxygen ions can be increased to such a level that this "sweep off" effect can be observable. However, the main effect of collisions of ionospheric ions with the Xe gas is the formation of the unstable (beam) ion velocity distribution resulting in the generation of low-hybrid plasma oscillations. The produced ion beam is very inhomogeneous in space. We can estimate the beam density (a fundamental parameter governing the conditions of instability) assuming that the main contribution to the beam density at a distance R is provided by the ions scattered at $r < R$ and $t \approx R/v_T$.

Thus, we have

$$\frac{n_b}{n_i} = \frac{\bar{N}_i}{n_i v_{sc} R^2} = \frac{\langle n_i v\rangle}{n_i v_{sc}} \frac{\sigma dN_{Xe}}{v_T R^2 dt} R$$

$$= \frac{\sigma dN_{Xe}}{v_T R dt} = \frac{60}{R}.$$

For $R \le 10^4$, we obtain $n_b/n_i \sim 10^{-3}$–10^{-4}.

Heating of Electrons

The acceleration or heating of electrons by waves during the development of the ion–ion instability is usually considered as a substantial element in the chain of processes resulting in anomalous ionization in the rarefied medium. An estimate of the typical mean free path of ionospheric electrons at elastic collisions in the Xe cloud during elastic collisions (σ_e – Xe ~ (0.3–1) × 10^{-15}) at the density of neutrals yields [see formula (1)]

$$\lambda_{e-Xe} \approx 1/n_{Xe}\sigma_{e-Xe} \approx (1\text{–}3)r^2,$$

where the distance r from the injector (in meters) indicates that the elastic e–Xe collisions remain significant up to $r \sim 1$ m. At a distance $r > 3$ m, collisions of electrons are too rare to change their dynamics or distribution. According to our previous consideration, the density of plasma ions scattered on Xe atoms is rather high for $r \le 3$ m, and ion acoustic oscillations can be generated in this region, resulting in strong heating of electrons (which is possible when they are trapped and their trajectories intersect in the wave potential). We can estimate the energy of accelerated electrons assuming that the ion–ion instability is stabilized by trapping ions in the potential well φ_{trap}. Then, the electron gains an additional energy $\varepsilon \sim e\varphi_{trap} = m_i v dv = 3 \pm 5$ eV, where dv is the velocity shift between the beam and wave. Thus, heating of electrons to energies higher than the ionization potential is possible only due to a resonant interaction with significantly longer waves in a significantly greater volume.

The reflected ions form a *bump-on-tail* distribution near the injector, and an ion–ion instability becomes possible, since the relative velocity V_b between the ionospheric plasma and beam ions significantly exceeds the thermal velocity of background plasma ions. The ion acoustic instability is suppressed in the ionosphere at $T_e \approx T_i$, and the quasi-potential low-hybrid oscillations remain the main source of instability during their resonance interaction with the ion beam $kv_b \approx k_\perp V_b \approx -\omega_{pe} = \omega_c(-k_z/k)$ (where ω_{pe} and ω_c are the Langmuir and electron cyclotron frequencies, respectively). We suppose that $\omega \ll \omega_c$ and the wave number k_z (parallel to the magnetic field) is smaller than the $k_\perp$ wave number (perpendicular to this field). In accordance with [6], we calculate the local growth rate of the ion beam instability assuming that the length of the unstable wave is smaller than the diameter of the ion cloud

$$\gamma_b = \omega \frac{\omega_{pi}^2}{1 + (\omega_p/\omega_c)^2}\left(\frac{1}{k\Delta V_b}\right)^2\left(\frac{n_b}{n_i}\right) \sim \omega\left(\frac{n_b}{n_i}\right) \ge 10^2,$$

where ΔV_b is the velocity variance in the beam equal to $\sim 1/2V_b$ in our case.

The threshold of the ion–ion instability is determined by the period during which the wave escapes from the region of interaction with the beam. This quantity can be represented in terms of an effective

damping rate $\nu = V_{gz}/R$, where V_{gz} is the group wave velocity $V_{gz} = \partial\omega/\partial k_z = \omega/k_z$. The necessary condition of instability $\gamma_b \geq \nu$ is satisfied at $k_z R \geq n_i/n_b \approx 10^3$.

Above this threshold, the instability is saturated due to the quasi-linear resonant interaction between electrons and low-hybrid waves. If the equilibrium is attained and a balance between the wave growth and damping is reached, we can determine (see [9]) the distribution of electrons accelerated by the ion beam instability according to the equation $(\gamma_b + \gamma_e)W_k = 0$. Here, W_k is the energy density of waves, and γ_e is the Landau damping expressed as

$$\gamma_e = \omega \frac{\omega_{pe}^2}{k^2(1 + (\omega_{pe}/\omega_c)^2)} \frac{\partial F_e}{\partial v_{ez}}\bigg|_{v_z k_z = \omega}$$

at a resonance $\omega = k_z v_{ez}$ with magnetized electrons.

With the aid of the equation

$$\frac{\partial F_e}{\partial v_{ez}} = -\frac{\gamma_b}{\omega}\frac{k_*^2[1 + (\omega_{pe}/\omega_e)^2]}{\omega_{pe}^2} \simeq -\left(\frac{m_e}{m_i}\right)\frac{1}{\Delta V^2}\frac{N_p}{N_{Xe}} \quad (4)$$

we obtain the solution representing a universal distribution of accelerated electrons $F_e(v_z) \propto v_{max} - v_z$ or $F_e(v_z) = 2(n_{supra}/n_0)(v_{max} - v_z)$ with

$$\frac{n_{supra}}{n_0} = \left(\frac{m_e}{m_i}\right)\frac{v_{max}^2}{\Delta V^2}\frac{N_p}{2N_{Xe}}.$$

The maximum velocity reached by electrons accelerated by waves is determined by the condition

$$v_{max}^2 = D_{zz}\tau = D_{zz}L_\parallel/v_{max},$$

where

$$D_{zz} = \omega_{pe}^2 \int \left(\frac{k_z}{k_\perp}\right)^2 \frac{E_k^2}{4\pi n m_e}\delta(\omega - k_z v_{ez})dk_z d(\pi k_\perp^2)$$

is the coefficient of electron diffusion in the velocity space. Further, we use an estimate

$$D_{zz} = v_{Te}^2\omega_{pe}^2\frac{W}{nT_e}\left\langle\left(\frac{k_z}{k_\perp}\right)^2\right\rangle\frac{1}{\omega} \approx v_{Te}^2\omega\frac{\omega_{pe}^2}{\omega_e^2}\frac{W}{nT_e},$$

where the wave energy $W = \int (E_k^2/4\pi)dk_z d\pi k_\perp^2$, and both the integral and the relation $k_\perp = k_\perp(k_z)$ are calculated along the spectrum line. We now can estimate the energy of accelerated electrons

$$\frac{\varepsilon_{max}}{T_e} \approx \left(\frac{L_\parallel}{v_{T_e}}\omega\frac{\omega_{pe}^2}{\omega_e^2}\frac{W}{nT_e}\right)^{2/3} \approx 10\text{–}20.$$

The calculations for typical parameters $W/nT_e \approx 10^{-3}$, $\omega_{pe}^2/\omega_e^2 \approx 10$, $L_\parallel \approx 10^6$ cm, $\omega \approx (0.3\text{–}1) \times 10^5$, and $T_e \approx 0.3\text{–}0.5$ eV show that the electron energy can be sufficient for the xenon ionization.

Xe Ionization by Accelerated Electrons

The suprathermal electrons accelerated by the low-hybrid turbulence additionally ionize Xe, and the rate of this ionization can be estimated using the calculated electron distribution as it was done in the case of impact ionization by plasma electrons [see formula (2)]:

$$\frac{dN_{Xe^+}}{dt} = \int\sigma_{eion}(v)F_e(v)dv\int n_{Xe}dV \approx \langle\sigma_{eion}n_e v\rangle N_{Xe},$$

$$\frac{1}{t_{ion}} = \frac{d\log N_{Xe^+}}{dt} \sim \frac{1}{3}\sigma_{eion}(v_{max})n_{supra}v_{max}$$

$$\approx 6\times 10^{-16}n_0\left(\frac{m_e}{m_i}\right)\frac{v_{max}^3}{\Delta V^2}\frac{N_p}{6N_{Xe}}$$

$$\approx 10^{-16}v_{max}n_0\frac{m_e v_{max}^2}{m_i\Delta V^2}\frac{N_p}{N_{Xe}} \approx 10^{-5}.$$

Here, $m_e v_{max}^2/m_i\Delta V^2 \approx 0.3\text{–}1$ and $N_p/N_{Xe} \approx 10^{-2}$. Thus, in ~1000 s of neutral Xe injection, only 1% of atoms will be ionized.

CONCLUSIONS

Our theoretical study has shown the following:

(1) In spite of the very small amount of the injected neutral Xe, a sufficient number of "seeded" energetic ions (both newly produced Xe and scattered ionospheric ions) arise due to collisions with the background plasma.

(2) We can expect the development of the ion–ion instability of low-hybrid waves at distances $r \sim 3\text{–}100$ m. In the vehicle reference system, the wave phase velocity component perpendicular to the magnetic field is within the range of the reflected ion velocities 0–7 km/s. However, the wave group velocity is directed almost along the magnetic field, and the waves can reach a satellite and can be detected.

(3) At the quasi-linear interaction, the low-hybrid wave accelerates electrons along the magnetic field to suprathermal energies. At a favorable direction of the magnetic field, these electrons can reach the vehicle and can be detected.

(4) The expected flux of these electrons and the number of their collisions with the neutral xenon is insufficient to increase the plasma density.

Apparently, these conclusions agree with the observational data presented and can explain them. Unfortunately, the lack of data on the low-frequency (low-

hybrid) wave activity and spectra of energetic electrons makes it impossible to realize a complete pattern of the phenomenon and to draw final conclusions.

REFERENCES

1. Alfvén, H., *On the Origin of the Solar System*, Oxford: Oxford Univ. Press, 1954.
2. Galeev, A.A. and Chabibrachmanov, I.C., The Critical Ionization Phenomenon in Astrophysics, *Proc. Joint Varenna–Abastumani Int. School and Workshop on Plasma Astrophysics*, Lominadze, D., Ed., 1986, pp. 129–136.
3. Haerendel, G., Alfvén's Critical Velocity Effect Tested in Space, *Z. Naturforsch.*, 1982, vol. 34a, pp. 728–735.
4. Marshall, J.A., Burch, J.L., Choueiri, E.Y., and Kawashima, N., CIV Experiment on *ATLAS-1*, *Geophys. Res. Lett.*, 1993, vol. 20(6), pp. 499–502.
5. Haerendel, G., Kelley, M.C., and Pfaff, R.F., Electric Field Measurements during the Condor Critical Velocity Experiment, *J. Geophys. Res*, 1986, vol. 91, no. A9, pp. 9939–9946.
6. Mikhailovskii, A.B., *Teoriya plazmennykh neustoichivostei. T. 1. Neustoichivosti odnorodnoi plazmy* (Theory of Plasma Instabilities. Vol. 1. Instabilities of Homogeneous Plasma), Moscow: Atomizdat, 1971.
7. Papadopoulos, K., On the Physics of the Critical Ionization Velocity Phenomena, *Space Plasma Physics*, Trieste: Plasma Physics College, 1985, pp. 33–58.
8. Torbert, R.B., Review of Critical Velocity Experiments in the Ionosphere, *Adv. Space Res.*, 1990, vol. 10, pp. 47–58.
9. Oraevskii, V.N., Volokitin, A.S., and Lizunov, G.V., Whistler Wave Generation by the Transversally Limited Ion Beam, *Fiz. Plazmy*, 1995, vol. 20, issue 5, pp. 91–95.